International Journal of Heat and Mass Transfer 71 (2014) 779–789

Contents lists available at ScienceDirect

International Journal of Heat and Mass Transfer

journal homepage: www.elsevier.com/locate/ijhmt

Determining the thermal conductivity of liquids using the transient hot disk method. Part I: Establishing transient thermal-fluid constraints

Ronald J. Warzoha, Amy S. Fleischer *

Department of Mechanical Engineering, Villanova University, Villanova, PA 19085, United States

ARTICLE INFO

Article history:
Available online 20 November 2013

Keywords:
Transient hot disk
Onset of natural convection
Thermal conductivity
Thermal diffusivity
Fluids
Nanofluids
Numerical simulation
FLUENT

ABSTRACT

Methods to determine the thermal conductivity of liquids have come under increased scrutiny recently due to their relative importance in determining the precise physical mechanisms responsible for heat flow in different materials and at multiple length scales. In transient-based systems, one important but often overlooked parameter is the onset of natural convection. In the first part of this study, the transient effects of natural convection are analyzed numerically for a relatively new transient thermal characterization system (transient hot disk) in order to determine when they begin to affect the calculation of a surrounding fluid's thermal conductivity. A comprehensive analysis of the effect of a fluid's pertinent thermophysical properties, Rayleigh number and Prandtl number on the sensor temperature response during testing is completed. Subsequently, a correlation is developed to determine the onset of natural convection during testing for fluids having a wide range of Prandtl numbers. The solution is verified using experimentation with multiple fluids having known, temperature-dependent volumetric heat capacities. The correlation is used as part of a new method to accurately calculate the thermal conductivity of different Newtonian fluids in Part II of this study, which is published separately.

1. Introduction

Measuring the thermal conductivity of fluids is critically important for the development of novel thermal management systems [1–3] and for understanding the physics of complex fluids, such as nanofluids [4–6]. However, the reported thermal conductivities of these fluids vary widely among research groups using different thermal characterization techniques. This is particularly troublesome in the area of nanofluids [7–10], where an inaccurate measurement can result in a significant misrepresentation of the dominant thermophysics at different length scales within the fluid.

In order to illustrate the difficulty in measuring the thermal properties of fluids, it is useful to discuss the current state of research within the subject of nanofluids. In this area, the variation among reported values of effective thermal conductivity is significant and may be due to a variety of factors, including: the surface conditions of the nanostructures suspended in each fluid [11–15], the fluid's pH [16–19], the differences among measurement techniques [20–22] and liquid layering at the nanostructure interface [23]. A recent study attempted to establish a benchmark of the thermal conductivity of different types of nanofluids in an effort to definitively explain the thermophysical mechanisms that dominate heat transfer in homogenously distributed suspensions [24]. In this study, nearly 20 research groups evaluated the thermal conductivity of nanofluids that were synthesized in the same facility, thereby eliminating the differences between the physical, chemical and geometrical conditions of the nanoparticles used. Consequently, the only remaining difference among the measurements of thermal conductivity is the thermal characterization technique used. In the aforementioned study, the guarded hot plate, transient hot wire and transient hot disk techniques were used to measure the thermal conductivity of the nanofluid samples. Results suggest that there is a statistically significant deviation between the data obtained using each of the different measurement techniques, with considerable outliers in nearly all sample sets. The authors did not report the conditions (i.e. experimental run times, equipment geometries, etc.) used to determine the thermal conductivity in each case. One possible cause for this discrepancy, then, is that the onset of natural convection occurred at a time prior to the end of the test in one or more of the transient systems. Though some studies do exist to provide guidelines for avoiding natural convection in some transient-based systems [25–27], none allow the user to quantify when convection occurs based on pertinent fluid and system parameters, and thus users are currently unable to avoid its influence during experiment with great certainty. A number of other studies have confirmed that natural convection plays a significant role in the accuracy of different transient-based thermal characterization systems and have determined this to be one of the major factors that has fueled the ongoing debate over

* Corresponding author.
E-mail address: amy.fleischer@villanova.edu (A.S. Fleischer).

0017-9310/$ - see front matter © 2013 Elsevier Ltd. All rights reserved.
http://dx.doi.org/10.1016/j.ijheatmasstransfer.2013.10.064

the influence of nanoparticles on the thermal enhancement of common heat transfer fluids [20–22]. The results of the work done in these studies [20–22] suggest that natural convection, which is encountered when experimental run times are 'too long' or sensor power levels are 'too high', results in artificially high thermal conductivities. However, no criteria for the determination of this time as a function of pertinent experimental parameters (such as the fluid's Prandtl number) currently exist. Thus, in order to establish an accurate and repeatable solution method to use for measuring liquid thermal conductivity with transient thermal characterization techniques, it is critical to determine the maximum allowable experimental run time for each type of test as a function of all relevant experimental parameters.

The transient hot disk method is emerging as a primary tool for the measurement of the thermal conductivity of novel materials [16,17,28–33] due to its multiple advantages over other transient thermal characterization techniques. In fact, the transient hot disk method is represented in approximately 8% of the studies on the thermal conductivity of nanofluids as of 2010 [20], while less than 5% used steady-state techniques. Steady-state techniques, while simple and cost-effective to implement, require extremely careful preparation in order to avoid high measurement uncertainties, require very long run times and do not have the ability to maintain a precise fluid temperature. Transient techniques, on the other hand, have fast measurement times and can maintain a constant fluid temperature during testing. The most commonly used method, the transient hot-wire technique, is also cost-effective and has been well studied since its inception in 1931 [34]. However, its measurement capabilities are also limited. The platinum hot wire, for instance, is both expensive and brittle. Thus, it is extremely difficult to measure the thermal conductivity of adhesives, fluids with large Prandtl numbers, fluids in extreme temperature environments and nanofluids without risk of damage to the sensor during sample handling and testing. In order to measure the thermal conductivity of these types of materials without risk of damage to the equipment, research groups have increasingly turned to the transient hot disk system. In addition to being a robust and rapid thermal characterization method, the transient hot disk apparatus is able to determine both the thermal diffusivity and thermal conductivity of fluids and solids, which are important to characterize for materials used in transient applications (such as thermal energy storage materials [35–37]).

The transient hot disk technique, like the transient hot-wire technique, utilizes a volume element (sensor) that serves as both a heat source and a temperature sensor. The sensor must be fully immersed in a fluid or sandwiched between two solid samples in order to measure thermal conductivity. In principle, when the sensor is powered, its temperature will increase rapidly when immersed or sandwiched between insulating materials and increase slowly for thermally conductive materials. A detailed formulation of the solution for the thermal conductivity of fluids using the transient hot wire technique can be found in [38], while a detailed formulation of the solution for the thermal conductivity of materials using the transient hot disk can be found in [39] and the second part of this study [40]. While many studies have utilized the transient hot disk method to measure the thermal conductivity of solid materials [41–48], fewer have used this method to characterize the thermal conductivity of liquids [49–52]. Some of the studies on liquid phase thermal conductivity with the hot disk technique highlight the difficulty in taking measurements due to the possibility that natural convection occurs during testing [49,50], while others ignore these potential effects altogether [51,52]. In an effort to limit the presence of natural convection during testing, some researchers [49,50] have taken to substantially reducing measurement times and sensor power levels. However, this too can lead to inaccuracies in measurement, as such short sampling times may exaggerate the effects of the interfacial thermal resistance between the sensor and the fluid, and low power levels often lead to high rates of data scattering, resulting in artificially high thermal conductivities. A careful examination of these phenomena is given in the second part of this study [40] in order to determine optimal experimental run times during which natural convection is absent.

Though attempts have been made to avoid natural convection during testing with the transient hot disk system, few groups have compiled any quantitative data that illustrates the potential effect that it may have on calculating thermal conductivity. In a recent study, Nagai et al. [53] compared the measurements of the thermal conductivity of silicone oils using the hot disk method in both a microgravity environment and a 'ground-based' environment. Their results indicate that the measurements were greatly affected by the presence or absence of convection during testing, particularly for low Prandtl number fluids. More recently, Boumaza and Redgrove [49] evaluated the effect of natural convection on the calculated thermal conductivity of water and silicone oil when the hot disk sensor face was perpendicular to the direction of gravity. The authors found that Rayleigh–Benard convection currents increased with increasing sensor diameter, indicating that the Rayleigh number has a significant effect on the onset of convection in fluids. However, their work realistically represents a sensitivity study, and no effort was made to determine when convection occurs across the face of the sensor as a function of the thermophysical properties of the fluid and the power loading level of the sensor. In their conclusion, the authors comment that using a smaller sensor size can reduce the onset of significant natural convection, but that "for liquids it is clear that further development of the probe or measurement technique is required to obtain greater accuracy". Ultimately, no criteria currently exist to determine the time at which convection will occur as a function of sensor size, sensor power level and fluid type.

In an effort to reduce the uncertainty of the transient hot disk thermal characterization technique, a correlation for the onset of natural convection across a conventional hot disk sensor of varying diameter is developed in the first part of this study. This correlation is developed as a function of the surrounding fluid's thermal expansion coefficient, its Prandtl number, the Rayleigh number and the sensor power load via numerical simulation and experiment. Numerical simulation is performed using FLUENT (v. 12). The effect of sensor temperature rise during the measurement on the calculated thermal conductivity of the fluid is also examined due to the potential for the liquid to heat up rapidly in close proximity to the sensor face. In the second part of this study [40], an iterative solution procedure is developed using the correlation for the onset of natural convection that is established in this portion of the study and is verified using fluids with a wide range of Prandtl numbers.

2. Problem formulation

In this analysis, a thin circular disk is vertically immersed in a fluid with known thermophysical properties at an initial temperature, T_0 = 303.15 K. The circular element used in this study has a radius r = 3.189 mm and a thickness t = 0.01 mm, which represents a standard sensor size available for thermal characterization with the hot disk method. The radius remains unchanged in the numerical simulations. The strength of natural convection as represented by the Rayleigh number (Eq. (1)) is varied by changing the sensor power. In order to determine the effect of Ra, Pr (Eq. (2)) and thermal expansion coefficient (β) on the time to natural convection, each parameter is varied in a parametric analysis. The Prandtl number ranges from 0.7 to 1324 to represent a wide range of heat transfer fluids. Likewise, the coefficient of thermal expansion, β, varies from 0.0001 to 0.003 1/K. The heating power applied to the sensor disk varies between 0.05 and 0.25 W in order to create the *Ra* ranges for each fluid as given in Table 1. The thermophysical properties used to obtain each Prandtl and Rayleigh number are listed in Table 1.

$$Ra = \frac{g\beta QD^2}{k\nu\alpha} \tag{1}$$

$$Pr = \frac{c_p\mu}{k} = \frac{\nu}{\alpha} \tag{2}$$

$$\alpha = \frac{k}{\rho c_p} \tag{3}$$

In Eqs. (1)–(3), g is the force of gravity acting in the y-direction (m/s^2), β is the thermal expansion coefficient (1/K), Q is the sensor power level (W), D is the diameter of the hot disk sensor (m), k is the thermal conductivity of the surrounding fluid (W/m K), ν is the kinematic viscosity of the surrounding fluid (m^2/s), α is the thermal diffusivity of the surrounding fluid (m^2/s), c_p is the specific heat capacity of the surrounding fluid (J/kg K) and ρ is the density of the surrounding fluid (kg/m^3).

3. Numerical methods

Numerical simulations are the primary method used to determine the time to the onset of natural convection in the hot disk system as a function of *Ra*, *Pr* and β in this study. Numerical simulations are used to solve for the time to the onset of natural convection because it allows the user to alter the thermophysical properties of liquids in ways that cannot be done via experiment. For instance, numerical simulations allow the user to change the value of a fluid's thermal expansion coefficient without inherently altering its other thermophysical properties. Thus, the effect of each parameter on the resulting solution can be isolated. This type of parametric analysis is impractical in experimentation. However, whenever possible, experimentation is used to verify the results of the numerical simulations.

3.1. User-defined solution settings

The convergence criteria represents the minimum percent difference in the solution (pressure, momentum, temperature) obtained between iterations for all nodes in the simulation domain. This parameter is often changed to enhance the accuracy between simulation and experiment. For this analysis, the convergence criteria were set to 10^{-4} for momentum and 10^{-8} for energy. Additionally, the Boussinesq approximation is used due to the expectation that the temperature variation within the fluid is moderate for the fluids of interest in this study.

Under-relaxation factors allow the user to control the deviation in each solution for pressure, momentum and temperature at every node between successive iterations. In this way, the under-relaxation factors can both prevent divergence and reduce simulation time simultaneously. For this investigation, the under-relaxation factors were altered as a function of Prandtl number in order to aid convergence. Each of the under-relaxation factors used for this study is listed in Table 2.

The Courant number is an important parameter to define in order to obtain an accurate solution in transient simulations; if the Courant number is too large, for instance, the solution behaves as if the flow were compressible. The Courant number (in one dimension) is given in Eq. (7).

$$Co = \frac{u\Delta t}{\Delta x} \tag{4}$$

In Eq. (7), u represents the fluid velocity, Δt represents the time step and Δx is the distance between nodes. In transient free convection, it is often difficult to determine the fluid velocity *a priori*. Thus, the time step is reduced until convergence for the continuity equation is satisfied. The time step for each simulation is listed in Table 2 as a function of Prandtl number.

Upon decreasing the time step increment for each Prandtl number listed in Table 2, no discernable difference in the results was found.

3.2. Mesh independence

In order to ensure that the computational model accurately captures the effects of the model geometry, a mesh independence study is performed. In this study, the same geometry is used for all simulations. Thus, only one assessment of mesh independence is performed and is consequently valid for the rest of the simulations completed in this study. The results of the mesh independence test are presented in Table 3. This analysis is done using glycerol as the heat transfer fluid and with a heat load of 0.15 W as the applied power to the sensor. The initial temperature used for the mesh independence study is 310.15 K.

An unstructured mesh was used in this study in order to avoid the poor quality and face alignment produced when using a structured mesh for the circular disk. The computational model and domain mesh are shown in Fig. 1(a) while the disk mesh is shown in Fig. 1(b).

The solution was considered independent of the mesh at 69,645 nodes due to the negligible difference in the average temperature and average convection coefficient of the disk as a function of time (less than 1% difference between subsequent solutions over the entire duration of the simulation). Additionally, it was found that the computational domain was large enough to avoid the effects of the system boundaries on the transient temperature of the sensor. The entire computational domain was 10.16 cm × 2.54 cm × 5.08 cm. Thus, the total computational domain is at least an order of magnitude larger than the each corresponding sensor dimension.

3.3. Verification of the numerical solution via experiment

Once consistency is established, accuracy must be confirmed through experimentation. For experimental validation of the numerical solution, a transient hot disk apparatus (TPS 500, ThermTest) is used to measure the average temperature rise in the disk element as a function of time (t) and power load (Q). The sensor disk features a 10 μm thick double-spiral nickel foil wire encapsulated in a 25 μm thick Kapton foil forming a sensor disk of r = 3.189 mm. A DC power source is used to power the spiral nickel foil wire, resulting in Joule heating due to the electrical

Table 1
Thermophysical properties used to obtain different Prandtl and Rayleigh numbers.

Prandtl number	k (W/m K)	ρ (kg/m^3)	c_p (J/k K)	$\nu \times 10^{-6}$ (m^2/s)	Range of Rayleigh numbers
0.7	0.0271	1.127	1005	16.97	181–27,190
4.4	0.623	993	4180	0.66	32,448–4.87 × 10^6
204	0.249	1116	2387	19.12	22,232–6.66 × 10^5
1324	0.6025	3600	1172	189	123–18,416

Table 2
User-defined solution settings.

Prandtl number	Pressure relaxation factor	Momentum relaxation factor	Temperature relaxation factor	Body forces relaxation factor	Time step (s)
0.7	0.3	0.6	1	1	0.0001
4.4	0.3	0.8	0.9	1	0.0001
203.6	0.3	0.8	0.9	1	0.0001
1324	0.3	0.8	0.9	1	0.00001

resistance of the wire. The temperature rise in the sensor is recorded using a Wheatstone bridge.

In the first part of this study, the sensor disk is immersed in one of three heat transfer fluids: deionized water, glycerol or cupric sulfate. The thermal properties of each fluid at 310.15 K, including the Prandtl number, can be found in Table 4. Ethylene Glycol, also shown in Table 4, is used in the second part of this study [40] for broader verification of the methods used here.

The heat transfer fluids are confined in a cylindrical vessel with a radius of 13.04 mm and a height of 16.68 mm. The container is made from oxygen-free high conductivity copper (OFHC) and is partially immersed in a constant temperature bath filled with a 50/50 mixture of deionized water and ethylene glycol. Oxygen-free high conductivity copper was chosen as the container material due to its well-defined and exceptionally high thermal conductivity, which is designed to keep the sample fluid within the container at the same temperature as the external thermal bath prior to testing. In Fig. 1, the temperature of the fluid within the vessel is monitored as a function of its radius at the centerline. Fig. 1 shows results for DI water and Glycerol and demonstrates that no significant thermal stratification occurs within the fluid prior to testing. All other fluids within this study exhibit a thermal stratification that is between the ranges that were found for DI water and Glycerol at each bath temperature. The apparatus and vessel dimensions (including the thermocouple locations corresponding to Fig. 2) used for experimentation are shown in Fig. 3.

The sensor disk is vertically inserted into a thin slot in the container vessel and the sensor is thus fully immersed in the heat transfer fluid within the container. The container is then suspended in a constant temperature batch such that the bath fluid cannot enter into the sample container. The thermal bath is fixed at a temperature of 310.15 K for the deionized water and glycerol tests and at 305.15 K for the cupric sulfate tests. Two different initial temperatures were used here in order to illustrate that the initial temperature of the fluid does not affect the accuracy of the numerical solution as compared to experiment.

To initiate the experiment, a power of 0.15 W is applied to the sensor disk and the Wheatstone bridge is activated. The sensor temperature is recorded at a frequency of 20 Hz and the data is collected for a total of 10 s. The resulting transient temperatures for both the numerical and experimental analyses are shown in Figs. 4–6.

In Figs. 4–6, the temperature obtained by numerical simulation is shown to match the experimental data to within 1% across all simulation times. As shown in Table 4, the three heat transfer fluids span a wide range of Pr, Ra and β. The Prandtl and Rayleigh numbers span nearly four orders of magnitude, while the thermal expansion coefficient ranges from 2.52×10^4 to 7.24×10^4. Thus, the numerical simulation is considered to be accurate for the range of parameters (Pr, Ra, β) defined in this study.

4. Results and discussion

4.1. Transient temperature profile

A visualization of the transient thermal gradient across the vertically oriented hot disk sensor immersed in a fluid is presented in this section as a function of Rayleigh number, the fluid's Prandtl number and thermal expansion coefficient. The temperature gradient across the disk as a function of time is used to qualitatively analyze the effect of the system parameters on the transient heat transfer from the surface of the disk to the fluid.

The transient temperature across the hot disk is shown in Fig. 7 as a function of time for constant thermal expansion coefficient and power loading levels ($\beta = 0.0005$ 1/K, $Q = 0.15$ W). The surrounding fluid temperature at time $t = 0$ is set to 303.15 K.

In Fig. 7(a)–(c), it is evident that the transient thermal response of the vertical disk greatly depends on each fluid's Prandtl number. Additionally, the thermal profiles reveal the relative importance between conduction and convection. When buoyancy is negligible and conduction is dominant, the thermal profile across the vertical disk is constant as a function of y. However, when buoyant flow develops and is no longer negligible, the transient thermal profile shifts in the direction of the fluid flow (i.e. in the positive y direction). One can see this phenomena occur in Fig. 7(a)–(c) as the disk temperature in the y direction becomes 'uneven'. The point at which there is a transition from an 'even' temperature to an 'uneven' temperature is therefore considered to be the point at which natural convection begins.

Fig. 7(a)–(c) also serve to illustrate the differences in the time scales during which convection is active. For instance, it takes relatively little time for fluids with low Prandtl numbers (like air or water) to generate convective motion, whereas it takes significantly longer to reach this condition as the Prandtl number is increased. This indicates that run times are not as critical in fluids with high viscosities. This explains the results of [49], in which the thermal conductivity of silicone oil obtained by the hot disk sensor closely matched that obtained by steady-state and THW methods, whereas when water was used as the working fluid, it did not.

4.2. Time to the onset of convection

In order to achieve a high degree of accuracy when measuring the thermal conductivity of a solid or fluid with the transient hot disk, convection must be avoided for the entire duration of experimentation [39,49,50]. At experimental run times that include natural convection over the sensor face, the calculated thermal conductivities are artificially high. Therefore, this distinction is critically important, particularly in emerging fields (like nanofluids) that require accurate experimental thermal property measurements in order to correctly determine the dominant physics governing heat flow within the fluid. However, while it is important to avoid natural convection during measurement, when convection does not occur, longer measurement times result in greater accuracy. Thus, the optimal measurement time is that which is long enough to approach but not exceed the time to the onset of natural convection. Given the emerging importance of this transition, this study determines the time required to reach natural convection across a hot disk sensor and thus optimizes the accuracy of the measurement system.

In order to determine this transition point, the energy equation is solved for a thin vertical disk with a conduction boundary

Table 3
Results of the mesh independence study.

Total number of nodes	Time = 1 s maximum temperature (K)	Time = 1 s average h (W/m^2 K)	Time = 5 s maximum temperature (K)	Time = 5 s average h (W/m^2 K)	Time = 10 s maximum temperature (K)	Time = 10 s average h (W/m^2 K)
8749	312.99	827	316.43	427	318.85	324
14,905	312.90	886	315.98	483	318.37	359
30,409	312.77	956	315.58	538	317.90	396
69,645	312.53	1010	314.87	577	316.99	422
116,076	312.54	1012	314.83	582	316.95	426

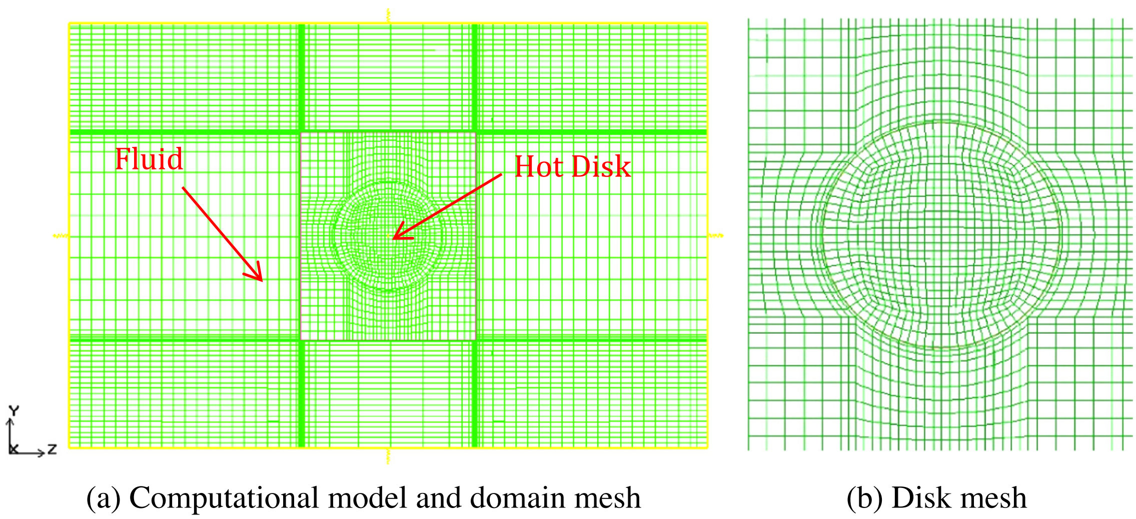

Fig. 1. (a) Computational model and domain mesh (y–z plane), (b) Disk mesh (y–z plane).

Table 4
Properties of the fluids used for experimentation and numerical simulation.

Fluid type	k (W/m K)	ρ (kg/m^3)	c_p (J/kg K)	ν (m^2/s)	β (1/K)	Prandtl number	Ra at 0.15 W
Deionized water [54]	0.623	993	4180	0.66×10^{-6}	3.71×10^{-4}	4.38	3.6×10^5
Cupric sulfate [54]	0.6025	3600	1172	1.89×10^{-4}	2.52×10^{-4}	1.32×10^3	927
Glycerol [54]	0.2855	1260	2479	1.12×10^{-3}	7.24×10^{-4}	1.23×10^4	1.4×10^3
Ethylene glycol [54]	0.2588	1102	2475	9.09×10^{-6}	3.19×10^{-3}	96.97	8.5×10^5

condition (i.e. convection is neglected). The solution to the energy equation represents the average temperature of the disk as a function of time. Once this solution is obtained, it is compared to the solution determined by numerical simulation. Numerical simulations are used to model the transient heat transfer phenomena in this study because they allow for facile alteration of the thermal properties of fluids without having to change other parameters. Thus, the user can isolate the effect of a single parameter, such as the thermal expansion coefficient, without changing the other fluid properties.

In this study, the point at which the numerical distributions begin to deviate from the analytical conduction solution represents the point at which convection begins. He [39] previously solved the energy equation for the vertical disk with constant heat generation and a conductive boundary condition. A portion of this derivation is given in Eqs. (5) and (6).

$$\alpha \cdot \nabla^2 T + \frac{Q}{\rho \cdot c_p} = \frac{\partial T}{\partial t} \tag{5}$$

Equation (5) represents the simplest form of the governing equation for heat transfer in a solid material with heat generation. When the boundary condition is that of a conductive, semi-infinite solid and the heat source is assumed to be equivalent to a point source, the solution to the general equation for an infinitely thin disk-shaped object becomes:

$$T(r,t) = T_0 + \frac{Q/\rho \cdot c_p}{(4\pi\alpha t)^{3/2}} \cdot exp\left(-\frac{r^2}{4\alpha t}\right) \tag{6}$$

In order to determine the point at which convection begins, the intersection between the solution to Eq. (6)and the transient solution for which convection is not considered to be negligible (obtained by numerical simulation) is found. An example of the method used to determine the transition point for a fluid with $Pr = 4.4$ and $Ra = 66{,}697$ is given in Fig. 8.

In Fig. 8, asymptotic distributions are shown for four different coefficients of thermal expansion. These distributions represent normalized convective curves (h/Q^*A) and are used to determine the time at which buoyancy begins to affect the temperature of the disk (i.e. the onset of natural convection). In this study, natural convection is considered to 'begin' when the convection curve for a fluid deviates from the distribution representing a solid with

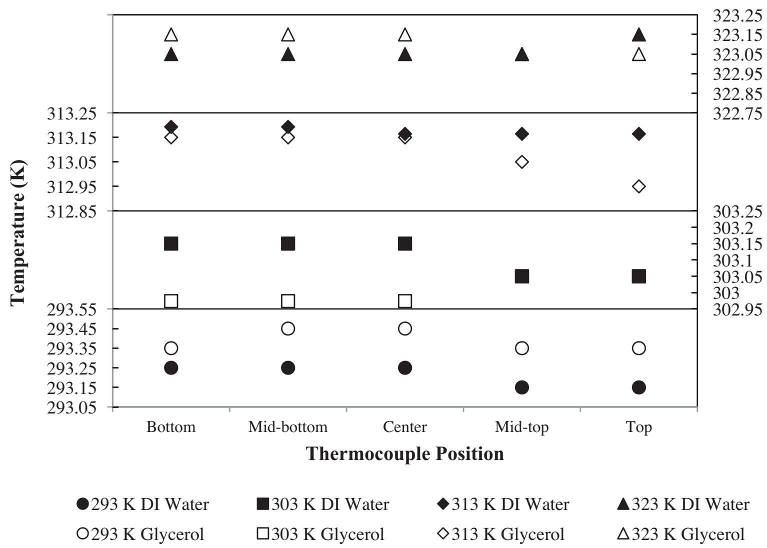

Fig. 2. Temperature of fluids within vessel as a function of radial coordinate.

equivalent thermophysical properties by 2%. This criterion was determined by comparing the analytical conduction solution to the solution for the numerical model when the disk was surrounded by a solid with equivalent thermophysical properties. These results matched to within 1% for all fluids and at all times. Thus, a 2% difference between the analytical conduction solution and the numerical model describing the sensor temperature when surrounded by a fluid is used. Using this criterion, one can determine when convection begins. In Fig. 8, for example, the convective curve representing the fluid having a thermal expansion coefficient of 0.0005 1/K begins to experience natural convection at $t = 10.3$ s. Fig. 8 also reveals that the onset of natural convection occurs more rapidly as the thermal expansion coefficient is increased. Additionally, as time increases, a steady-state convective condition is shown to exist across the disk.

In this study, IBM SSPS (Statistical Product and Service Solutions) Statistics Package v. 20 is used to apply a step-wise, non-linear, multi-variable regression technique to the data in order to determine the time to the onset of natural convection as a function of Rayleigh number, Prandtl number, power loading level and volumetric coefficient of thermal expansion. For this analysis, it is assumed that the data take the form of an asymptotic solution in accordance with Fig. 8. The Levenberg–Marquardt iteration method is used to determine the solution with the data obtained in the

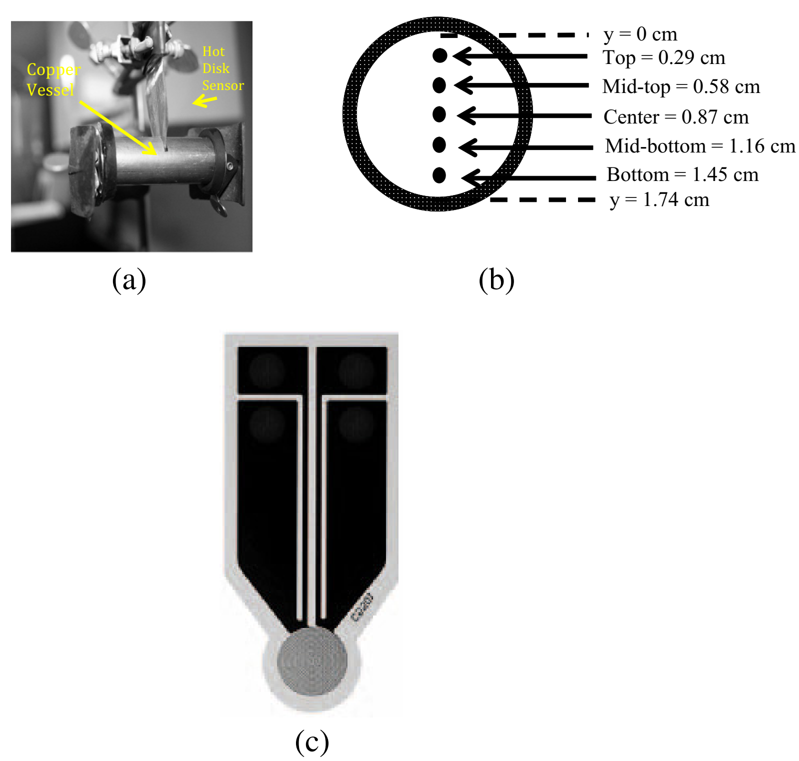

Fig. 3. (a) Apparatus used for comparing numerical and experimental transient thermal profiles across the transient hot disk sensor, (b) Vessel dimensions, (c) Hot disk sensor [55].

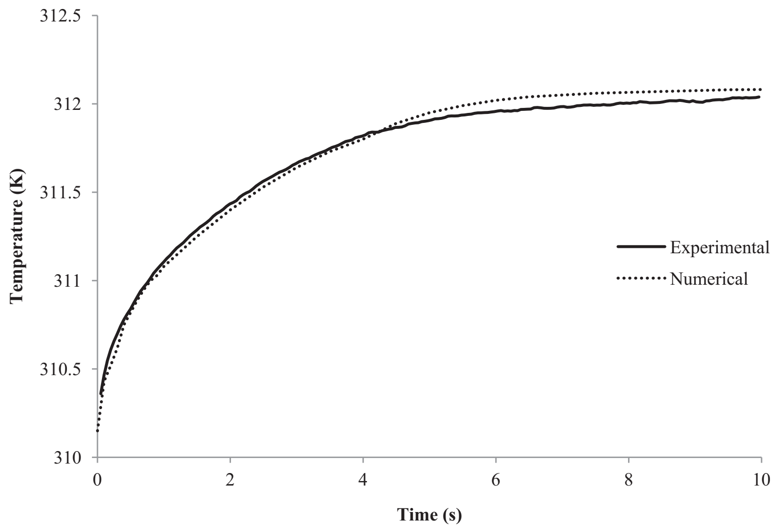

Fig. 4. Average transient temperature over the disk using deionized water as the heat transfer fluid ($Q = 0.15$ W).

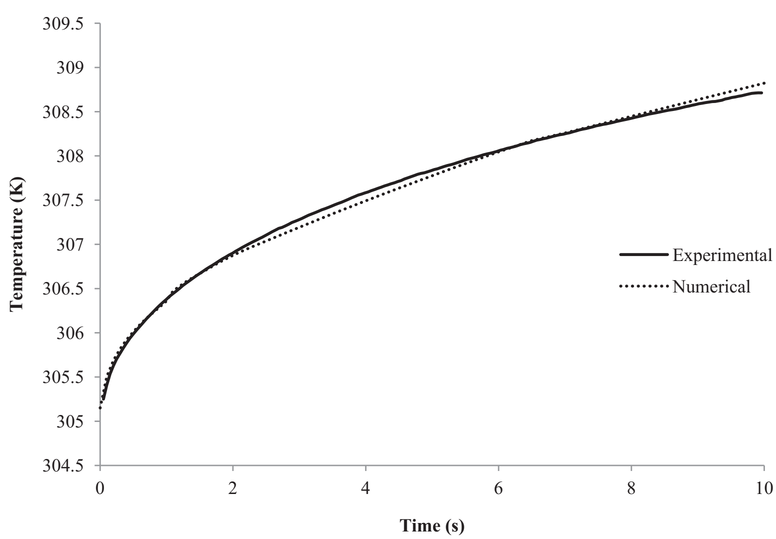

Fig. 5. Average transient temperature distribution over the disk using cupric sulfate as the heat transfer fluid ($Q = 0.15$ W).

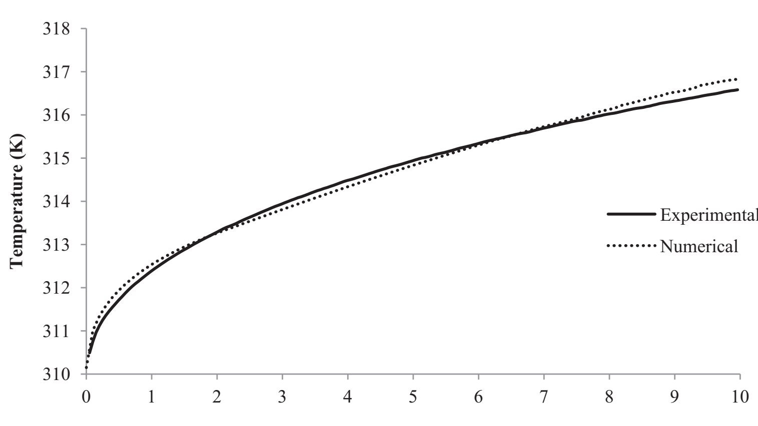

Fig. 6. Average transient temperature distribution over the disk using glycerol as the heat transfer fluid ($Q = 0.15$ W).

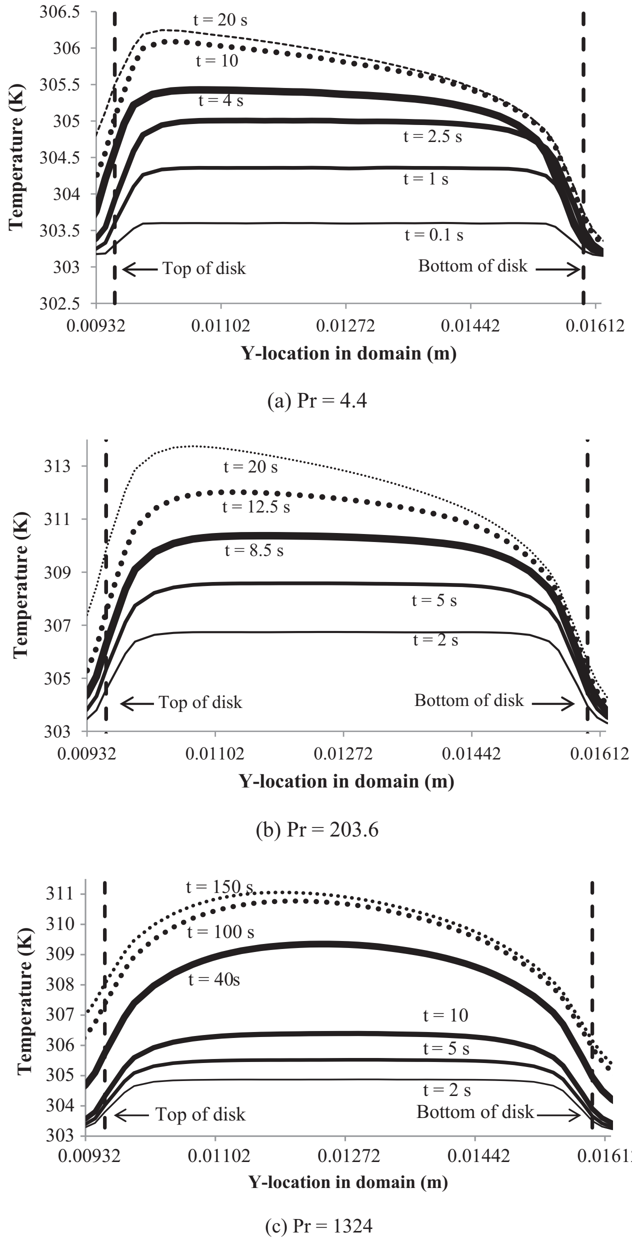

Fig. 7. Transient thermal profiles across the midpoint of the vertically oriented disk immersed in fluids with: (a) $Pr = 4.4$, (b) $Pr = 203.6$, (c) $Pr = 1234$. In all cases, $Q = 0.15$ W and $\beta = 0.0005$ 1/K.

numerical study, with a sum-of-squares convergence and parameter convergence of 1e−8. The result of this analysis is given in Eq. (7), which was verified using Prandtl and Rayleigh numbers not used in the determination of its solution.

$$t_{onsetCV} = (9.525e^{-6} \cdot \sec \cdot W^{0.791} \cdot K^{-0.830}) \cdot \left(\frac{Pr^{0.456} \cdot Ra^{0.285}}{Q^{0.791} \cdot \beta^{0.830}} \right) \qquad (7)$$

The solution for the onset of natural convection from the thin vertical disk given by Eq. (7) was found to match the data used for its calculation to within an average of 5.3%, with higher deviation at lower Prandtl numbers. Thus, Eq. (7) is found to be accurate to within 5.3% of the data for the range of Rayleigh and Prandtl numbers used to represent laminar flow in this study.

In order to verify the accuracy of Eq. (7), an experiment was done to determine the onset of natural convection at different temperatures using deionized water and matched to the solution of Eq. (7). Deionized water was chosen as the fluid for illustrative convenience: fluid's with low *Pr* were found to have rapid transitions from the point at which convection begins until steady-state convection is reached, which shortens the period over which mixed conduction/convection occurs. This helps to clearly distinguish between conduction and convection and thus serves to best illustrate the capabilities of Eq. (7). Additionally, as deionized water most often serves as the base fluid for nanofluids, it is of critical importance to maintain a diffusive regime during testing for many research groups, particularly because it is also a low *Pr* fluid (even in the presence of nanostructures). The results are shown in Fig. 9.

In Fig. 9, the transient temperature rise of the vertical disk surrounded by deionized water was obtained experimentally at a power loading level of 0.15 W and is plotted for five different fluid temperatures (293–333 K in 10 K increments). In this case, the fluid used was deionized water. The fluid was contained in the cylindrical copper vessel shown in Fig. 3 and its temperature was controlled by a thermal bath. For each fluid temperature, the time to the onset of convection was calculated using Eq. (7). In Fig. 9, steady-state convection begins when $dT/dt = 0$. It should be noted that there is a region of the solution where conduction and convection exist simultaneously. This is evident in Fig. 8, where the distribution representing $\beta = 0.003$ 1/K clearly departs from the conduction solution near $t = 5$ s, but does not reach a constant temperature difference (i.e. steady-state convection) until $t \sim 17$ s. The resulting solution from Eq. (7)represents the time to the *onset* of convection, and thus avoids the mixed conduction/convection regime altogether.

Given the high accuracy with which Eq. (7) predicts the onset of natural convection, users can now predict the thermal conductivity of liquids with confidence that natural convection does not influence the calculation. It should be noted that Eq. (7) is valid for Rayleigh numbers in the laminar flow regime. Thus, the disk size can be changed and the equation will remain valid so long as there exists laminar flow over the disk face. Additionally, the equation is valid for disk types that abide by the following constraint: the thermal settling time across the disk (t^2/α, where t is the disk thickness and α is the thermal diffusivity of the insulating layer around the double-spiral nickel foil wire) must be at least an order of magnitude lower than the total test time, as determined in [56]. Knowledge of this parameter is critically important for the measurement of the thermal properties of fluids using the hot disk sensor, which calculates their thermal conductivities by assuming a semi-infinite, conduction dominated boundary condition at both of its interfaces [39]. In this system, $t_{onsetCV}$ represents the maximum allowable run time for the experiment.

4.3. Effect of sensor temperature rise

In order to determine the sensitivity of the measurement technique to the temperature rise of the sensor, an experimental approach was used. For this aspect of the study, the hot disk sensor was immersed in Glycerol, whose thermal conductivity and diffusivity are well known [54]. The volumetric heat capacity, which can be obtained by dividing the thermal diffusivity by the thermal conductivity, was used in the solution for determining the thermal conductivity of the fluid using the hot disk sensor provided in [39] in order to avoid complex iteration. In order to evaluate the effect of temperature rise on the determination of the thermal conductivity using the hot disk sensor and the solution provided in [39], the sensor's power load was altered between runs (from 0.05 to 0.25 W). For this part of the study, the measurement times corresponded to ~0.2 s prior to the onset of natural convection obtained using Eq. (7). The results are shown in Fig. 10.

In Fig. 10, the vertical error bars represent the uncertainty in the system measurement when using the criteria for the onset of

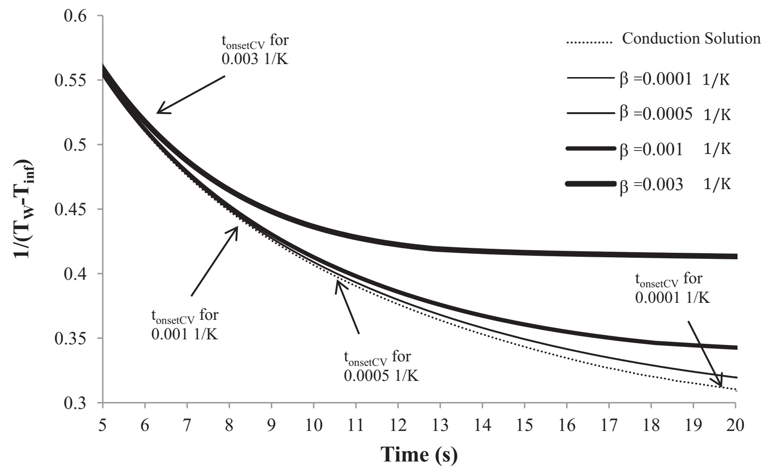

Fig. 8. Departure from conduction solution as a function of thermal expansion coefficient for a disk power loading level of 0.15 W.

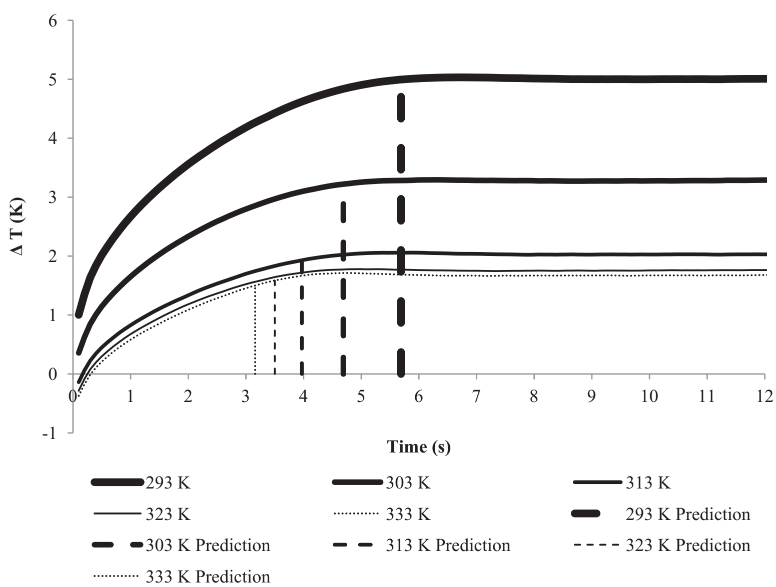

Fig. 9. Transient temperature rise of circular disk plotted (solid lines) and time to natural convection for each fluid temperature (dotted lines) for deionized water with $Q = 0.15$ W.

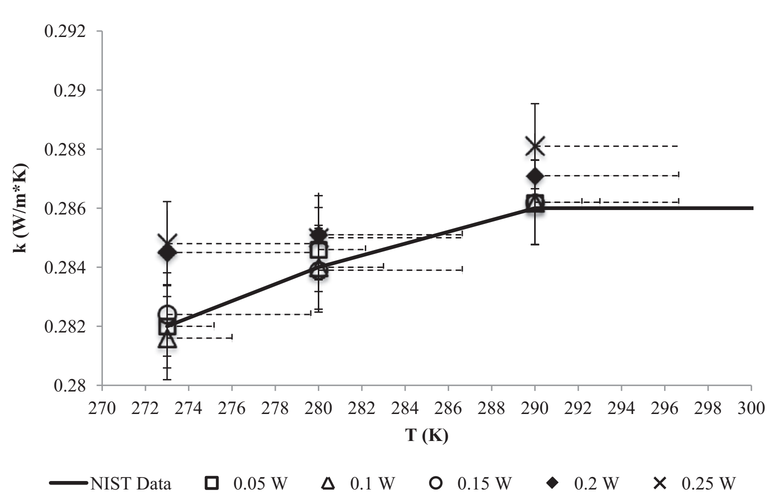

Fig. 10. Thermal conductivity of Glycerol as a function of sensor power loading level.

natural convection as the stopping point for the measurement of the thermal conductivity of Glycerol. In all cases, the uncertainty was within 0.5% of the reported thermal conductivity of Glycerol. The horizontal error bars in Fig. 10 represent the temperature rise of the sensor during measurement. It is clear from these results that as the temperature rise of the sensor increases (in correspondence with the sensor power load), the obtained thermal conductivity approaches that which has been reported in the literature for the sensor's upper temperature limit. For instance, when the thermal conductivity of Glycerol is measured at 280 K at low sensor power levels (0.05,0.1 W), the thermal conductivity is nearly identical to that which is reported in the literature. However, when the power level is increased (for instance, to 0.25 W), the calculated thermal conductivity is closer to the reported thermal conductivity at the upper limit of the sensor's temperature rise (287 K), with a notable exception being the case when the power loading level is 0.15 W. This observation was found to be consistent amongst all of the measurements. In accordance with the data, it is recommended that in order to obtain an accurate measurement of the thermal conductivity of a fluid at a given temperature (to within 2% of its actual value), a temperature rise of 5 K or less should be maintained during testing when measuring the thermal conductivity of fluids in increments of 10 K (or ½ of the measurement increment), else the user risk obtaining an artificially high thermal conductivity in much the same way that it is obtained when the user exceeds the time at which convection begins during measurement.

5. Conclusions

In this study, numerical simulations were used to determine the time to the onset of natural convection across the hot disk thermal constants analyzer sensor when oriented vertically and immersed in a fluid by varying pertinent system parameters (the fluid's Prandtl number, the Rayleigh number, the sensor power level and the fluid's thermal expansion coefficient). A non-linear regression technique was used to produce a correlation from the data in order to find the onset of natural convection across the hot disk sensor as a function of the aforementioned parameters. Experimental results agree to within 5.3% of the values produced by the equation used to calculate the onset of natural convection. Additionally, a sensitivity analysis was completed to determine the effect of the sensor temperature rise during testing on the calculation of the thermal conductivity of the surrounding fluid. It was found that the thermal conductivity of Glycerol showed statistically significant deviation from its reported value when a temperature rise greater than 5 K occurred during measurement. It was recommended that in order to accurately measure the thermal conductivity of a fluid at precise intervals over a range of temperatures, the sensor temperature should not exceed ½ of the intervals between fluid temperatures. These results are critically important for accurately determining the thermal conductivity of fluids using the transient hot disk system, which is experimentally illustrated in the second part of this study.

Acknowledgments

R.J.W. gratefully acknowledges support from the Environmental Protection Agency Science to Achieve Results (STAR) Fellowship.

This material is based upon work supported by the National Science Foundation under Grant No. 0931507. Any opinions, findings, and conclusions or recommendations expressed in this material are those of the author(s) and do not necessarily reflect the views of the National Science Foundation. The research described in this paper has also been funded in part by the United States Environmental Protection Agency (EPA) under the Science to Achieve Results (STAR) Graduate Fellowship Program. EPA has not officially endorsed this publication and the views expressed herein may not reflect the views of the EPA.

References

[1] N. Boerema, G. Morrison, R. Taylor, G. Rosengarten, Liquid sodium versus Hitec as a heat transfer fluid in solar thermal central receiver systems, Sol. Energy 86 (2012) 2293–2305.
[2] N. Anh Lai, M. Wendland, J. Fischer, Working fluids for high-temperature organic Rankine cycles, Energy 36 (2011) 199–211.
[3] R. Saidur, K.Y. Leong, H.A. Mohammed, A review on applications and challenges of nanofluids, Renewable Sustainable Energy Rev. 15 (2011) 1646–1668.
[4] W. Yu, S.U.S. Choi, The role of interfacial layers in the enhanced thermal conductivity of nanofluids: a renovated Maxwell model, J. Nanopart. Res. 5 (2003) 167–171.
[5] D.H. Kumar, H.E. Patel, V.R.R. Kumar, T. Sundararajan, T. Pradeep, S.K. Das, Model for heat conduction in nanofluids, Phys. Rev. Lett. 93 (2004) 144301–144304.
[6] C.H. Li, G.P. Peterson, Experimental investigation of temperature and volume fraction variations on the effective thermal conductivity of nanoparticle suspensions (nanofluids), J. Appl. Phys. 99 (2006) 084314.
[7] J.A. Eastman, S.U.S. Choi, S. Li, W. Yu, L.J. Thompson, Anomalously increased effective thermal conductivities of ethylene glycol-based nanofluids containing copper nanoparticles, Appl. Phys. Lett. 78 (2001) 718–720.
[8] P. Keblinski, R. Prasher, J. Eapen, Thermal conductance of nanofluids: is the controversy over?, J Nanopart. Res. 10 (2008) 1089–1097.
[9] X. Feng, D.W. Johnson, Mass transfer in SiO_2 nanofluids: a case against purported nanoparticle convection effects, Int. J. Heat Mass Transfer 55 (2012) 3447–3453.
[10] M. Chandrasekar, S. Suresh, A review on the mechanisms of heat transport in nanofluids, Heat Transfer Eng. 30 (2009) 1136–1150.
[11] R.L. Vander Wal, S.D. Mozes, V. Pushkarev, Nanocarbon nanofluids: morphology and nanostructure comparisons, Nanotechnology 20 (2009) 105702.
[12] T.T. Baby, S. Ramaprabhu, Investigation of thermal and electrical conductivity of graphene based nanofluids, J. Appl. Phys. 108 (2010) 124308.
[13] N. Jha, S. Ramaprabhu, Synthesis and thermal conductivity of copper nanoparticle decorated multiwalled carbon nanotubes based nanofluids, J. Phys. Chem. C. 112 (2008) 9315–9319.
[14] L. Chen, H. Xie, Surfactant-free nanofluids containing double- and single-walled carbon nanotubes functionalized by a wet mechanochemical reaction, Thermochim. Acta 497 (2010) 67–71.
[15] Z. Talaei, A.R. Mahjoub, A.M. Rashidi, A. Amrollahi, M. Emami Meibodi, The effect of functionalized group concentration on the stability and thermal conductivity of carbon nanotube fluid as heat transfer media, Int. Commun. Heat Mass Transfer 38 (2011) 513–517.
[16] X.F. Li, D.S. Zhu, X.J. Wang, N. Wang, J.W. Gao, H. Li, Thermal conductivity dependent pH and chemical surfactant for Cu–H_2O nanofluids, Thermochim. Acta 469 (2008) 98–103.
[17] X.J. Wang, D.S. Zhu, S. Yang, Investigation of pH and SDBS on enhancement of thermal conductivity of nanofluids, Chem. Phys. Lett. 470 (2009) 107–111.
[18] M.E. Meibodi, M. Vafaie-Setfi, A.M. Rashidi, A. Amrollahi, M. Tabasi, H.S. Kalal, The role of different parameters on the stability and thermal conductivity of carbon nanotube/water nanofluids, Int. Commun. Heat Mass Transfer 37 (2010) 319–323.
[19] E.V. Timofeeva, D.S. Smith, W. Yu, D.M. France, D. Singh, J.L. Routbort, Particle size and interfacial effects on thermo-physical and heat transfer characteristics of water-based α-SiC nanofluids, Nanotechnology 21 (2010) 215703.
[20] G. Paul, M. Chopkar, I. Manna, P.K. Das, Techniques for measuring the thermal conductivity of nanofluids: a review, Renewable Sustainable Energy Rev. 14 (2010) 1913–1924.
[21] C.H. Li, W. Williams, J. Buongiorno, L.-W. Hu, G.P. Peterson, Transient and steady-state experimental comparison study of effective thermal conductivity of Al_2O_3/water nanofluids, J. Heat Transfer 130 (2007) 042407.
[22] S.A. Putnam, D.G. Cahill, P.V. Braun, Z. Ge, R.G. Shimmin, Thermal conductivity of nanoparticle suspensions, J. Appl. Phys. 99 (2006) 084308.
[23] P. Keblinski, S.R. Phillpot, S.U.S. Choi, J.A. Eastman, Mechanisms of heat flow in suspensions of nano-sized particles (nanofluids), Int. J. Heat Mass Transfer 45 (2001) 855–863.
[24] J. Buongiorno, D.C. Venerus, N. Prabhat, T. McKrell, J. Townsend, R. Christianson, et al., A benchmark study on the thermal conductivity of nanofluids, J. Appl. Phys. 106 (2009) 094312.
[25] R. Rusconi, W.C. Williams, J. Buongiorno, R. Piazza, L.-W. Hu, Numerical analysis of convective instabilities in a transient short-hot-wire setup for measurement of liquid thermal conductivity, Int. J. Thermophys. 28 (2007) 1131–1146.
[26] R. Rusconi, L. Isa, R. Piazza, Thermal-lensing measurement of particle thermophoresis in aqueous dispersions, J. Opt. Soc. Am. B. 21 (2004) 605–616.
[27] F. Shen, J.M. Khodadadi, Combined thermocapillary and buoyancy-driven convection within short-duration pulse-heated liquid droplets, Numer. Heat Trans. A-Appl. 36 (1999) 839–857.

[28] G.H. Zhang, C.Y. Zhao, Thermal and rheological properties of microencapsulated phase change materials, Renewable Energy 36 (2011) 2959–2966.
[29] M. Anis-ur-Rehman, A. Maqsood, Measurement of thermal transport properties with an improved transient plane source technique, Int. J. Thermophys. 24 (2003) 867–883.
[30] G.A. Longo, C. Zilio, Experimental measurement of thermophysical properties of oxide-water nano-fluids down to ice-point, Exp. Therm. Fluid Sci. 35 (2011) 1313–1324.
[31] V. Goyal, D. Teweldebrhan, A.A. Balandin, Mechanically-exfoliated stacks of thin films of Bi_2Te_3 topological insulators with enhanced thermoelectric performance, Appl. Phys. Lett. 97 (2010) 133117.
[32] M. Shamsa, S. Ghosh, I. Calizo, V. Ralchenko, A. Popovich, A.A. Balandin, Thermal conductivity of nitrogenated ultrananocrystalline diamond films on silicon, J. Appl. Phys. 103 (2008) 083538.
[33] K. Kataoka, Y. Takahashi, N. Kijima, H. Nagai, J. Akimoto, Y. Idemoto, K.-I. Ohshima, Crystal growth and structure refinement of monoclinic Li_2TiO_3, Mater. Res. Bull. 44 (2009) 168–172.
[34] J.K. Horrocks, E. McLaughlin, Non-steady state measurements of thermal conductivities of liquids polyphenyls, Proc. R. Soc. Lond. 273 (1963) 259–274.
[35] A. Sari, A. Karaipekli, Thermal conductivity and latent heat thermal energy storage characteristics of paraffin/expanded graphite composite as phase change material, Appl. Therm. Eng. 27 (2007) 1271–1277.
[36] J.M. Khodadadi, S.F. Hosseinizadeh, Nanoparticle-enhanced phase change materials (NEPCM) with great potential for improved thermal energy storage, Int. Commun. Heat Mass Transfer 34 (2007) 534–543.
[37] O. Sanusi, R. Warzoha, A.S. Fleischer, Energy storage and solidification of paraffin phase change material embedded with graphite nanofibers, Int. J. Heat Mass Transfer 54 (2011) 4429–4436.
[38] Y. Nagasaka, A. Nagashima, Absolute measurement of the thermal conductivity of electrically conducting liquids by the transient hot-wire method, J. Phys. E. Sci. Instrum. 14 (1981) 1435–1440.
[39] Y. He, Rapid thermal conductivity measurement with a hot disk sensor. Part I. Theoretical considerations, Thermochim. Acta 436 (1–2) (2005) 122–129.
[40] R.J. Warzoha, A.S. Fleischer, Determining the thermal conductivity of liquids using the transient hot disk method. Part II: Establishing an accurate and repeatable solution method, in Press.
[41] S.A. Al-Ajlan, Measurement of thermal properties of insulation materials by using transient plane source technique, Appl. Therm. Eng. 26 (2006) 2184–2191.
[42] W.-L. Cheng, R.-M. Zhang, K. Xie, N. Liu, J. Wang, Heat conduction enhanced shape-stabilized paraffin/HDPE composite PCMs by graphite addition: preparation and thermal properties, Sol. Energy Mater. Sol. Cells 94 (2010) 1636–1642.
[43] L.-W. Fan, Y.-C. Hu, T. Tian, Z.-T. Yu, The prediction of effective thermal conductivities perpendicular to the fibres of wood using a fractal model and an improved transient measurement technique, Int. J. Heat Mass Transfer 49 (2006) 4116–4123.
[44] R. Coquard, E. Coment, G. Flasquin, D. Baillis, Analysis of the hot-disk technique applied to low-density insulating materials, Int. J. Therm. Sci. 65 (2013) 242–253.
[45] K. Kamran, M. Anis-ur-Rehman, A. Maqsood, Thermal and electrical properties of crystalline silver bromide, J. Phys. D. Appl. Phys. 40 (2007) 869–873.
[46] S. Mo, P. Hu, J. Cao, Z. Chen, H. Fan, F. Yu, Effective thermal conductivity of moist porous sintered nickel material, Int. J. Thermophys. 27 (2006) 304–313.
[47] Y. He, Rapid thermal conductivity measurement with a hot disk sensor: Part 2. Charterization of thermal greases, Thermochim. Acta 436 (2005) 130–134.
[48] P. Zhang, Y. Hu, L. Song, H. Lu, J. Wang, Q. Liu, Synergistic effect of iron and intumescent flame retardant on shape-stabilized phase change material, Thermochim. Acta 487 (2009) 74–79.
[49] T. Boumaza, J. Redgrove, Use of the transient plane source technique for rapid multiple thermal property measurements, Int. J. Thermophys. 24 (2003) 501–512.
[50] J. Nanda, C. Maranville, S.C. Bollin, D. Sawall, H. Ohtani, J.T. Remillard, J.M. Ginder, Thermal conductivity of single-wall carbon nanotube dispersions: role of interfacial effects, J. Phys. Chem. C 112 (2008) 654–658.
[51] S.Y. Wu, H. Wang, S. Xiao, D.S. Zhu, An investigation of melting/freezing characteristics of nanoparticle-enhanced phase change materials, J. Therm. Anal. Calorim. 110 (2012) 1127–1131.
[52] B. Wright, D. Thomas, H. Hong, L. Groven, J. Puszynski, E. Duke, X. Ye, S. Jin, Magnetic field enhanced thermal conductivity in heat transfer nanofluids containing Ni coated single wall carbon nanotubes, Appl. Phys. Lett. 91 (2007) 173116.
[53] H. Nagai, F. Rossignol, Y. Nakata, T. Tsurue, M. Suzuki, T. Okutani, Thermal conductivity measurement of liquid materials by a hot-disk method in short-duration microgravity environments, Mater. Sci. Eng. A-Struct. 276 (2000) 117–123.
[54] E.W. Lemmon, M.L. Huber, M.O. McLinden, NIST Standard Reference Database 23: Reference Fluid Thermodynamic and Transport Properties-REFPROP, Version 9.0, National Institute of Standards and Technology, Standard Reference Data Program, Gaithersburg, 2010.
[55] www.hotdiskinstruments.com, accessed: 4/4/13.
[56] V. Bohac, M.K. Gustavsson, L. Kubicar, S.E. Gustafsson, Parameter estimations for measurements of thermal transport properties with the hot disk thermal constants analyzer, Rev. Sci. Instrum. 71 (2000) 2452–2455.